ORIGINAL PAPER

Collapsibility deterioration mechanism and evaluation of compacted loess with sodium sulfate under drying–wetting cycles

Yongpeng Nie[1,2] · Wankui Ni[1,2] · Wenxin Tuo[1,2] · Haiman Wang[1,2] · Kangze Yuan[1,2] · Yang Zhao[3,4]

Abstract
The deterioration of loess collapsibility under drying–wetting cycles is one of the serious threats to the artificial loess slopes and foundations in China, especially when soluble salt is involved. In this paper, a series of collapsibility tests were used to study the collapsibility deterioration of compacted loess with sodium sulfate under drying–wetting cycles, and the scanning electron microscope (SEM) tests were carried out to investigate the variation in microstructural properties. The results show gradual increase in the collapsibility of the loess samples with the increasing drying–wetting cycles and salt content. The collapsibility coefficient increases and gradually tends to stabilize with the progress of drying–wetting cycles, while changes linearly or exponentially with the salt content. The coupling effect of drying–wetting and salt erosion makes the loess skeleton looser and weaker in structure, providing more pore space for the deterioration of collapsibility, and when the salt content is greater than 0.5%, the deterioration ratio due to salt erosion is higher than that of drying–wetting. By fitting the collapsibility deterioration data with the hyperbolic function, the effect of drying–wetting cycles and salt content on the maximum and development speed of deterioration rate are quantitatively analyzed, and then, an interpolation equation of collapsibility deterioration considering both the influencing factors is established, which can well evaluate the collapsibility deterioration of compacted loess.

✉ Wankui Ni
niwankui@chd.edu.cn

[1] College of Geological Engineering and Geomatics, Chang'an University, Xi'an 710054, China

[2] Key Lab of Western Geological Resources and Geoengineering under Ministry of Education, Chang'an University, Xi'an 710054, China

[3] State Key Laboratory of Geomechanics and Geotechnical Engineering, Institute of Rock and Soil Mechanics, Chinese Academy of Sciences, Wuhan 430071, China

[4] University of Chinese Academy of Sciences, Beijing 100049, China

1 Introduction

Loess is widely distributed in China, with a total area of about 640,000 km^2, accounting for more than 6% of the country's area, forming the famous Loess Plateau. (Luo et al. 2017; Wang et al. 2021a). Since its collapsibility can be effectively reduced or even eliminated after compaction (Kim and Kang 2013; Wang et al. 2011), loess is widely used as a construction material in the Loess Plateau region and plays an important role in the construction of high-fill subgrade, embankments and foundations (Feng et al. 2015; Xu et al. 2021). However, it is not uncommon to find cases of engineering geological disasters, such as landslides, building cracking and tilting, and settlement, caused by the re-emergence of collapsibility of compacted loess (Li et al. 2012). Therefore, the in-depth research on the collapsibility mechanisms of compacted loess has been the focus and difficulty in the field of geotechnical engineering.

It is well known that the collapsibility of loess is closely related to its microstructure (Li et al. 2016; Wang et al. 2019a), while the Loess Plateau is located in an arid semi-arid region, where the loess is subjected to repeated drying–wetting cycles due to climate change, such as high variability in rainfall, groundwater table, and surface evaporation (Kong et al. 2017; Zhang et al. 2020). The drying–wetting cycles alter the microstructure of the soil, such as soil particle size, shape and arrangement of soil particles (Ni et al. 2020), the type of pore structure (Lu et al. 2015), and the strength of inter-particle bonding (Pires et al. 2020), thus affecting the physical and mechanical properties of soil in different ways. Numerous studies have proved that the permeability, deformation and shear strength of loess will experience irreversible deterioration under drying–wetting cycles (Chou and Wang 2021; Hu et al. 2020; Malusis et al. 2011; Tripathy and Rao 2009), often more significantly than those caused by other climatic conditions, such as freezing–thawing (Kong et al. 2022). In the meantime, the influence of soluble salts on the loess collapsibility cannot be ignored. An increasing number of studies have shown that soluble salts dissolved in pore water increase the ion types and concentrations in the soil (Fan et al. 2017; Ying et al. 2021), thereby changing the water film thickness on the surface of loess particles (Yilmaz et al. 2008; Zhang et al. 2013) and the suction between loess particles (Shen et al. 2017; Xue et al. 2020), all of which will change the microstructure of loess to varying degrees and thus affect its collapsibility. What's more, the drying–wetting cycles can not only provide the driving force for the migration of soluble salts to the soil surface (Higuchi et al. 2015; Hu et al. 2019), but also cause the dissolution and crystallization of soluble salts, which negatively affects the structural strength of soil (Xu and Coop 2016), a process known as salt erosion (Ietto et al. 2018).

The above studies prove that the disturbances caused by both drying–wetting cycles and salt erosion and its influence on the collapsibility of compacted loess cannot be ignored; however, recent studies have rarely discussed this issue. In addition, although some scholars have developed mathematical models describing the deterioration process of strength parameters in order to study the relationship between soil strength and drying–wetting cycles or the content of soluble salts (Hossain Md et al. 2016; Xu et al. 2016), such as Scelsi et al. (2021) proposed an elastic–plastic model that can reproduce the behavior of unsaturated clays in saline environments in order to address the chemo-hydro-mechanical response of unsaturated compacted materials. However, the quantitative relationship between these two influencing factors and collapsibility has rarely been reported. The other, even more grim fact is that soil salinization on the Loess Plateau is becoming more and more serious today due to various factors such as agricultural irrigation, water

conservancy projects, and improper land management (Jin et al. 2019; Wang et al. 2019b; Zhang et al. 2019). Thus, for the engineering safety in loess areas, it is urgent to reveal the mechanism of collapsibility deterioration of saline compacted loess under drying–wetting cycles and present a quantitative interpolation equation.

To achieve these research objectives, saline compacted loess samples were prepared using different preset concentrations of sodium sulfate solutions in this study. The changes in particle, pore morphology and collapsibility of the samples after drying–wetting cycles were investigated by the double-oedometer test and SEM test. By analyzing the collapsibility coefficients under different influencing factors, a comprehensive collapsibility deterioration interpolation for compacted loess considering the salt content and the number of drying–wetting cycles was established, and the collapsibility deterioration mechanism under the coupling effect of drying–wetting cycles and salt erosion was revealed from the microscopic perspective. The research results provide a useful reference for engineering construction in the Loess Plateau region.

2 Materials and methods

2.1 Materials

The loess used in this study was taken from Huangling County (35° 39′ 51″ N, 109° 16′ 6″ E), Yan'an City, Shaanxi Province, China, as shown in Fig. 1. All loess were collected from 3 m below the ground surface, which belonged to Q_3 Malan loess. The basic physical properties of the loess were measured based on the Standard for geotechnical testing method GB/T 50123-2019 (Mohurd 2019), the particle size distribution curve of the loess (Fig. 2) was determined with the Bettersize 2000 laser particle size tester, and the ion content of the soluble salt in the loess was measured using neutralization titration and ion chromatography. The results are summarized in Table 1. Obviously, the soluble salt cations in the loess are mainly Na^+, and the anions are mainly SO_4^{2-}. It can therefore be inferred that the main component of loess soluble salt in this area is Na_2SO_4, but its initial content is extremely low, so the influence of initial content can be ignored when preparing samples.

2.2 Sample preparation

To simulate the actual engineering soil conditions more accurately, the dry density of loess samples in this study was set as 1.55 g/cm³, and the water content as 13%. In addition, four levels of salt content (S) of 0%, 0.5%, 1%, and 1.5%, that is, the percentage of the mass of Na_2SO_4 contained in the loess to the dry soil mass, were considered.

First, the collected loess was crushed and dried in an oven at 105 °C, then passed through a 2 mm sieve. Next, the loess was mixed with preset concentrations of sodium sulfate solution to reach the target water content (~ 13%), and then sealed in an airtight container for 7 days to achieve moisture homogenization. After that, the actual water content was measured by the weighting method (Xu et al. 2020) to ensure that the deviation from the target water content was not more than 0.2%. Finally, the prepared loess was placed into a mold (diameter $D = 61.8\,mm$ and height $H = 20\,mm$) for static compaction to obtain the compacted loess samples.
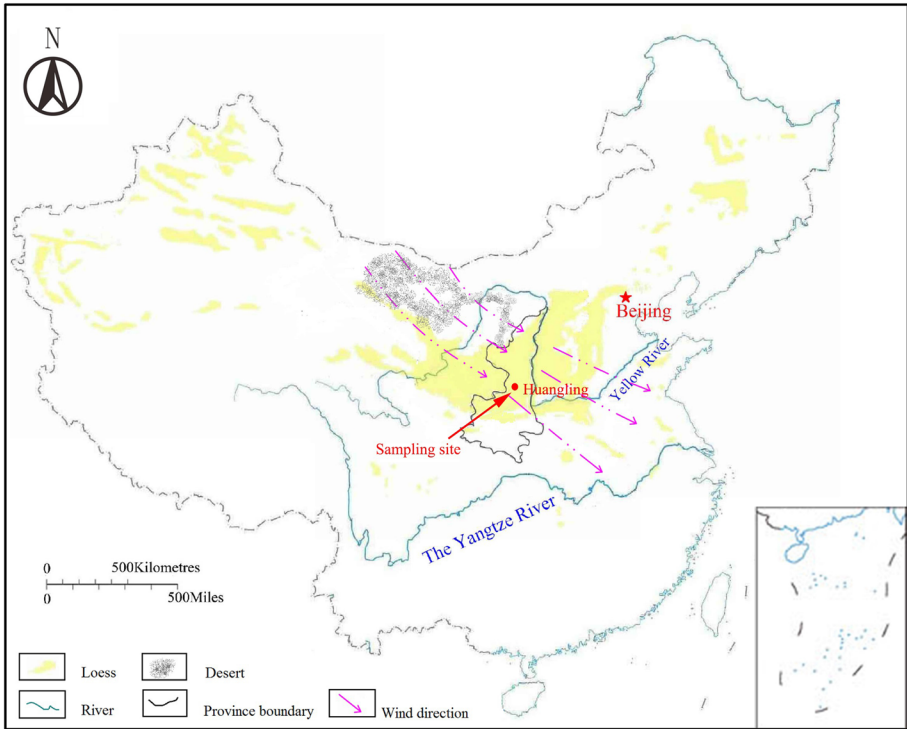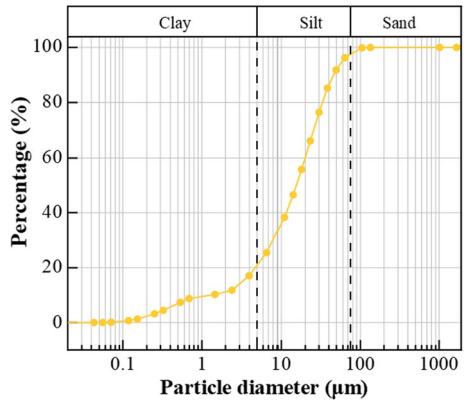
Fig. 1 Loess distribution and the sampling site (modified after: Zhang et al. 2018)

**Fig. 2** The particle size distribution curves for loess

2.3 Drying–wetting cycles process

To more accurately simulate the influence of drying–wetting cycles under natural conditions, drying–wetting cycles in this study include two processes: dehumidification and humidification, as shown in Fig. 3. The dehumidification process was realized by drying in a constant temperature blast drying oven at 45 °C (simulating the summer surface

Table 1 Basic physical indexes and initial ion content of loess samples

Property	Value
Maximum dry density ρ_d(g/cm^3)	1.72
Optimal water content w(%)	14.05
Specific gravity Gs	2.72
Liquid limit w_L (%)	29.1
Plastic limit w_P (%)	19.2
Particle size distribution (%)	
Sand > 0.075 mm	3.02
Silt 0.005–0.075 mm	79.94
Clay < 0.005 mm	17.04
Initial ion contents (mg/kg)	
Na^+	130.5
Ca^{2+}	87.44
K^+	6.86
Mg^+	53.99
SO_4^{2-}	246.43
CL^-	101.18
CO_3^{2-}	89.21
HCO_3^-	233.29

Fig. 3 Drying–wetting cycles applied to loess samples
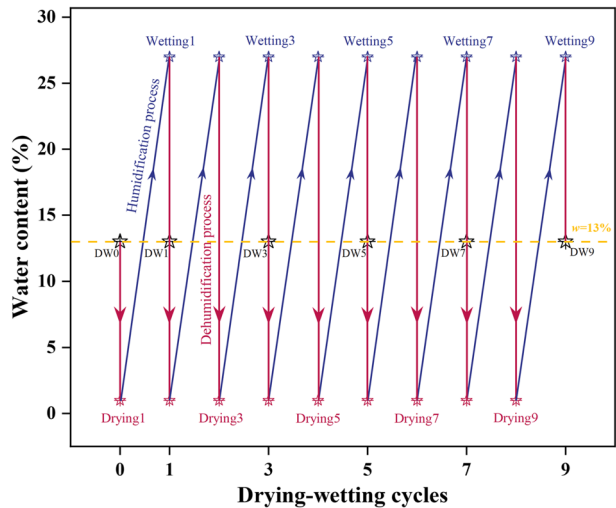
temperature), while the humidification process was completed by using a burette to evenly add distilled water from the top and bottom of samples. The water content of samples during dehumidification and humidification was determined by the weighting method. The measurement results showed that under the four considered salt contents, the loess samples reached a constant weight after being dried in an oven for 3 days (~ w = 1%) or humidified to 95% saturation (~ w = 27%). Thus, the upper and lower limits of water content during the drying–wetting cycles were controlled to 1 and 27%. It is worth mentioning

that during the humidification process, the required amount of distilled water was slowly dripped into the loess sample, and then, the sample was stored in a constant temperature and humidity chamber for 24 h, which could satisfy the uniform wetting condition from outside to inside. Therefore, the duration for the wetting process was controlled to 24 h. After experiencing preset drying–wetting cycles, i.e., $N=0$, 1, 3, 5 7 and 9, the loess samples were used for SEM tests and collapsibility tests.

Standard loess samples under five experimental conditions were used to verify the uniformity of water and salt in the soil, namely T_1 ($w=27\%$, $S=0.5\%$, $N=0$), T_2 ($w=27\%$, $S=1.0\%$, $N=0$), T_3 ($w=27\%$, $S=1.5\%$, $N=0$), T_4 ($w=27\%$, $S=0.5\%$, $N=3$) and T_5 ($w=1\%$, $S=0.5\%$, $N=3$). Each standard loess sample was divided into two cylindrical sections with height of 10mm. Each section was first dried with a portion of soil to measure the water content, while the remaining soil was air-dried and sieved through a 2-mm sieve. The leachate was prepared using distilled water at a soil to water ratio of 1:5. 50 ml of leachate was taken and filled into a beaker weighed before the test. It was dried on an electric stove, and the total mass of the beaker and sample was weighed every 0.5 h until the difference between the two consecutive mass values was less than 0.001 g, and then, the salt content of each section was calculated. The results showed that the maximum deviations of the measured data for loess samples with target water contents of 1 and 27% are 0.10 and 0.16%, which are negligible compared to the target for simplicity. Compared with the three target salt contents of 0.5–1.5%, the maximum differences were 0.013, 0.018 and 0.015%, respectively. The variation in salt content proves that the total soluble salts in each section is basically the same as that of Na_2SO_4 solution. Comparisons prove the homogeneity of the saline compacted loess samples at different test stages.

2.4 Experiment methods

2.4.1 SEM tests

The entire SEM testing process was divided into four main steps. During the first step, the loess sample as prepared above was cut into a 10 mm×10 mm×20 mm cuboid specimen from the center. The second step was to dry the cuboid specimen with a vacuum freeze dryer to remove the moisture, while the third step was to break apart the cuboid specimen from the middle, and stick the fresh section face up on the base with conductive tape. Lastly, sprayed gold on the specimen and used the Quanta 450 FEG Scanning Electron Microscope to observe and record the microstructure of sample.

2.4.2 Collapsibility tests

The double-oedometer test (Li et al. 2019) was used in this study to assess the collapsibility of loess samples. Based on this method, the collapsibility coefficient δ_s under certain applied loading is calculated by Eq. (1):

$$\delta_s = \frac{S_1 - S_2}{H_0} \tag{1}$$

where, S_1 represents the settlement due to the oedometer compression test where the sample is wetted to saturation (mm); S_2 denotes the settlement result from the oedometer

compression test at a constant initial moisture content (mm); and H_0 is the initial height of the sample (mm).

The collapsibility of loess can be classified according to the value of δ_s, that is: when $\delta_s < 0.015$, it is non-collapsible loess; when $0.015 \leq \delta_s \leq 0.03$, it is weakly collapsible loess; when $0.03 < \delta_s \leq 0.07$, it is moderately collapsible loess; when $\delta_s > 0.07$, it is strongly collapsible loess (Mohurd 2019).

Multiple WG triple high pressure consolidometer apparatuses were used for the Collapsibility tests. All samples were subjected to a series of increasing vertical pressure of 50, 100, 150, 200, 300, 400, 600 and 800 kPa. The stability standard under stress loading at each stage is that the settlement is less than 0.01 mm/h, and then, the next stage of load is applied after the settlement is stable.

3 Results

3.1 Collapsibility coefficient

Figure 4 shows the relationship between the compacted loess collapsibility coefficient, δ_s, and the vertical stress, p, obtained by the double-oedometer test. As shown in Fig. 4a, the δ_s of compacted loess samples not subjected to any drying–wetting cycles ($N=0$) are all less than the critical value of 0.015 at various pressures, that is, the fully compacted loess has negligible collapsibility. However, with an increase in the number of drying–wetting, the δ_s of samples under different stresses increase continuously. It is worth noting that after 9 cycles, the δ_s under 200 kPa stress is 0.015, which indicates that the compacted loess sample at this time appears secondary collapsibility, that is, the collapsibility coefficient of
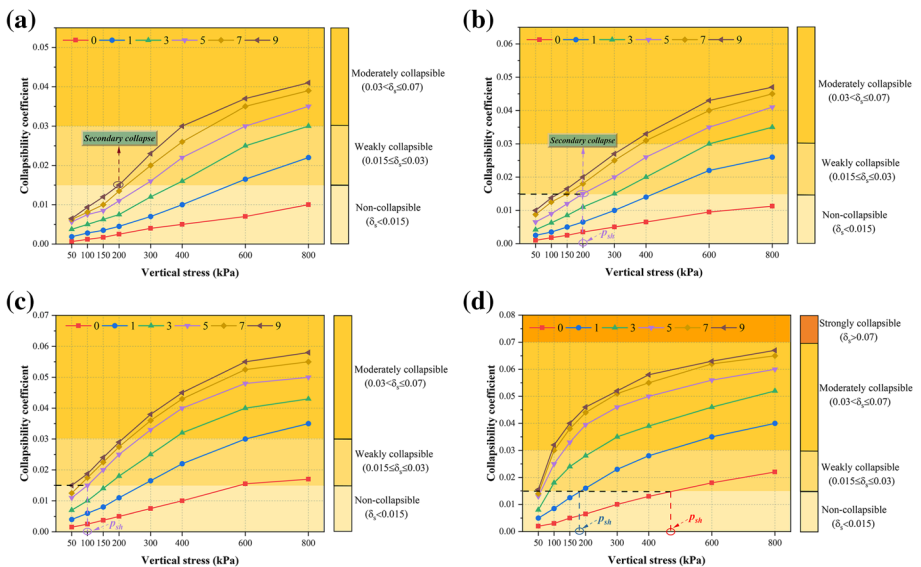

Fig. 4 Deterioration of collapsibility coefficient at different stress (a) S = 0% (b) S = 0.5% (c) S = 1% (d) S = 1.5%

densely compacted loess again reaches or exceeds the benchmark value for defining collapsibility (Li et al. 2018; Wang et al. 2020). While the number of drying–wetting required for secondary collapsibility of compacted loess with a salt content of 0.5% is 5 (Fig. 4b), meaning that an increase in salt content promotes the occurrence of secondary collapsibility. In addition, the initial collapse pressure, p_{sh}, is an important indicator reflecting the collapsibility of loess. It marks the beginning of collapsibility of loess, and the pressure value when the δ_s is equal to 0.015 is usually taken for this value. Comparing Fig. 4b and c, the value of p_{sh} under 5 drying–wetting drops from 200 to100 kPa when the salt contents of samples increase from 0.5 to 1%. And when the salt content of samples is 1.5%, the value of p_{sh} after undergoing 1 drying–wetting is significantly less than the value undergoing 0 cycle, as shown in Fig. 4d.

Usually, the collapsibility coefficient under 200 kpa pressure is used as the standard to quantitatively evaluate the collapsibility of loess in actual engineering construction, as shown in Fig. 5.

For compacted loess samples with different salt contents, their collapsibility coefficient increases as the number of drying–wetting increases, but the growth rate gradually decreases, showing a logarithmic trend (Fig. 5a). Taking compacted loess samples with 1% salt content as an example, the values of δ_s are 0.005, 0.011, 0.018, 0.025, 0.0275 and 0.029, respectively, at 0, 1, 3, 5, 7 and 9 cycles, showing an increasing trend, but the increases are 120%, 63.6%, 38.9%, 10% and 5.5%, showing a decreasing rate. For other loess samples with different salt contents (0, 0.5 and 1.5%), the collapsibility coefficient shows similar trends under the effect of drying–wetting cycles. In addition, it is worth noting that before the drying–wetting cycle ($N=0$), the change of the collapsibility coefficient with the salt content is not significant compared with that after the drying–wetting cycles (Fig. 5b). Nevertheless, with an increase in salt content when N > 0, the collapsibility coefficients increased significantly to varying degrees, showing an exponential trend. For example, for the compacted loess samples under 9 drying–wetting, compacted loess with a salt content of 0, 0.5, 1 and 1.5% corresponds to a δ_s of 0.015, 0.02, 0.029, and 0.046, respectively, with an increase of 33.3, 45 and 58.6%, showing an increasing trend, and that the collapsibility coefficient under other numbers of drying–wetting cycles also basically conform to this trend.

3.2 SEM images

Figure 6 illustrates the SEM images of compacted loess samples at ×1000 magnifications before and after drying–wetting cycles. The drying–wetting cycles promoted the
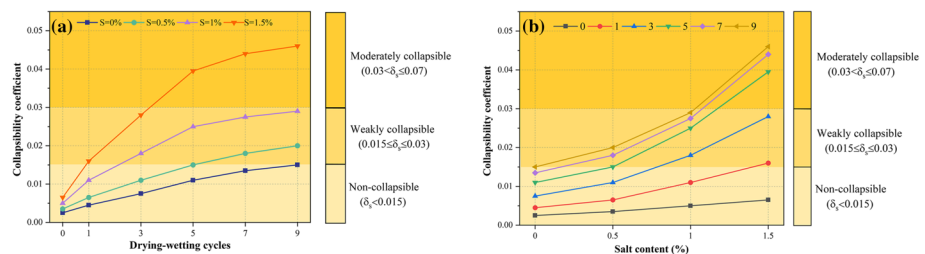
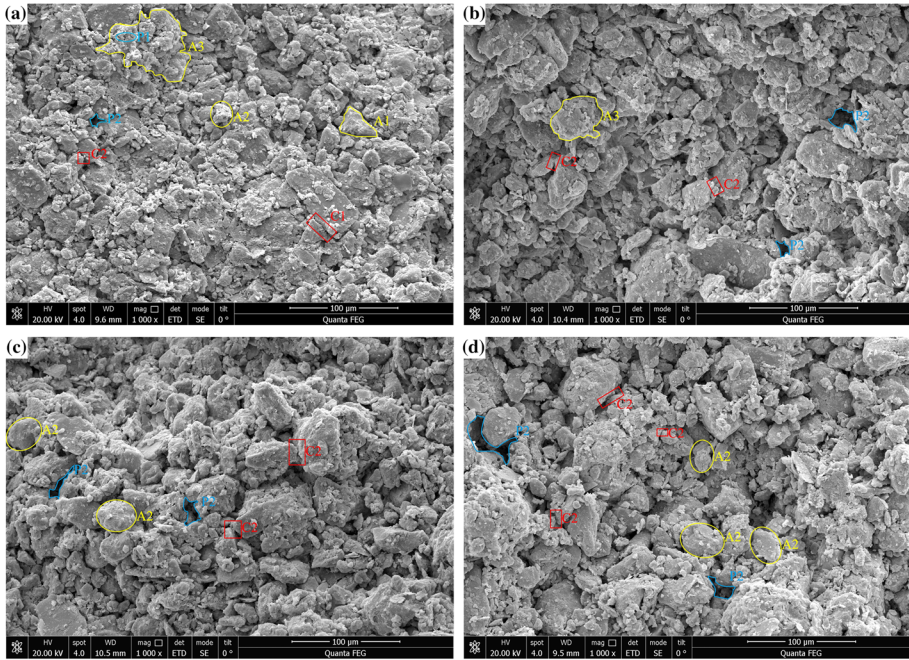**Fig. 5** Deterioration of collapsibility coefficient at 200 kPa (**a**)$\delta_s \sim N$ (**b**) $\delta_s \sim S$

Fig. 6 SEM images of samples after different drying–wetting cycles ($S = 0\%$) (**a**) $N = 0$ (**b**) $N = 1$ (**c**) $N = 3$ (**d**) $N = 7$. *Note* A1 angular particle, A2 round particle, A3 cemented aggregate; C1 face contact, C2 point contact; P1 intra-aggregate pore, P2 inter-aggregate pore

transition of particle type and interparticle contact type. It can be appreciated that the loess skeleton before cycles consists mainly of cemented aggregates and larger angular or round particles that are in point or face contact, with inter-aggregate and intra-aggregate pores co-existing. After one cycle, part of the cemented aggregates disintegrates, more inter-aggregate pores appear in the soil, the contact between particles weakens, and the skeleton tends to loosen. After three cycles, angular particles and inter-particle face contact decrease, and more round particles and point contact appear. After seven cycles, the contact between particles is mainly point contact, and soil pores are developed in main forms of inter-aggregate pores.

Figure 7 presents the SEM images of compacted loess samples at ×1000 magnifications with different salt contents. The loess skeleton is mainly composed of cemented aggregates and larger monomeric particles, and the increases in salt content aggravated the weakening of loess structure. At $S = 0.5\%$, the number of monomeric particles decreases and that of fragmented aggregates increase. At $S = 1\%$, the loess skeleton tends to be looser, and the number of particles covered by salt crystals grows. At $S = 1.5\%$, the loess structure is further loosened, and more particle contacts are damaged with more developed inter-aggregate pores.

The above SEM images were binarized, and pore identification was performed using the Pores and Cracks Analysis System (Liu et al. 2011), as shown in Fig. 8. The pore area and fractal dimension were selected to quantify the microscopic pore structure variation of the compacted loess samples.
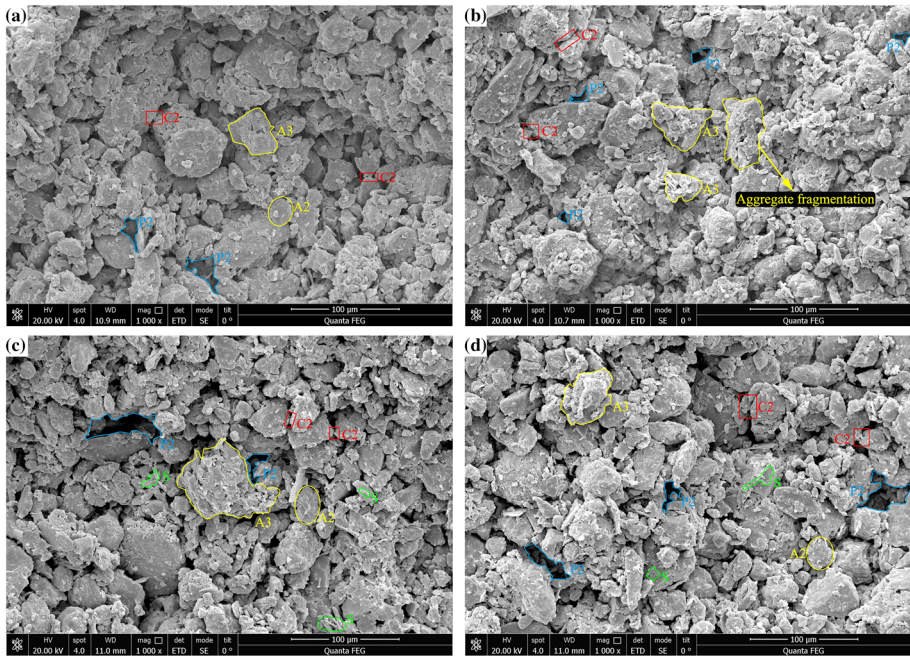
Fig. 7 SEM images of samples at different salt contents ($N = 9$) (**a**) $S = 0\%$ (**b**)$S = 0.5\%$ (**c**) $S = 1\%$ (**d**) $S = 1.5\%$. *Note* S salt crystal

Import the SEM image and binarize it
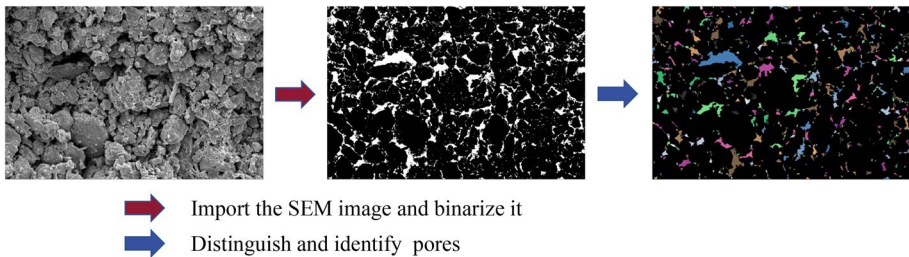
Distinguish and identify pores

Fig. 8 Binarization and pore identification of SEM image

According to the equivalent pore diameter, loess pores are divided into micropores ($d \leq 2$ μm), small pores ($2 \mu m < d \leq 8$ μm), mesopores ($8 \mu m < d \leq 32$ μm) and macropores ($d > 32$ μm) (Lei 1987). Then, Fig. 9 shows the pore area percentage and pore fractal dimension of the loess samples. One can see that with the increase of N and S, the area of macropores and mesopores increases, while the area of small pores and micropores decreases.

At $S = 0\%$, the area percentages of mesopores and macropores in the sample after nine cycles increase by 23.29 and 3.73%, while the area percentages of small pores and micropores decrease by 19.82 and 7.2%, respectively. Compared with before the drying–wetting cycles, the pore area percentages of samples after the cycle have changed significantly, mainly caused by the transition from micropores and small pores to mesopores and macropores. The increase in the ratio of mesopores and macropores enhances the
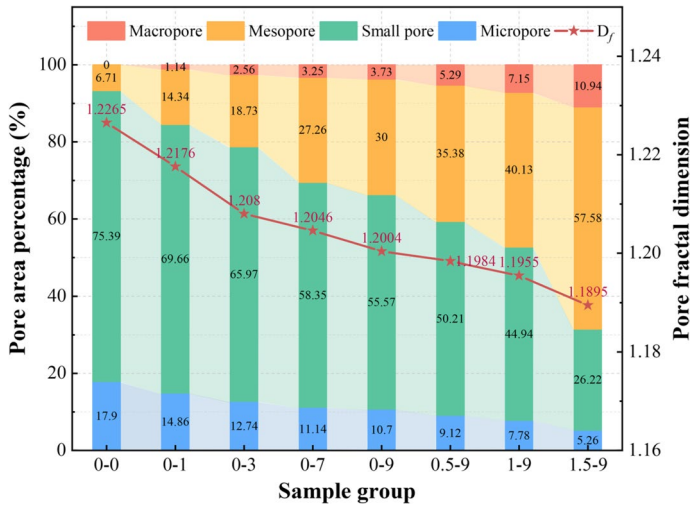
Fig. 9 Variation in pore area distribution and fractal dimension. *Note* The sample group, such as 0–7, signifies that the salt content is 0%, and the drying–wetting cycle is 7

connectivity of the pore structure of loess samples, and this phenomenon is especially evident for samples with higher salt content. In addition, the pore fractal dimensions of loess samples decrease after drying–wetting cycles, which indicates that the complexity of pore morphology in loess samples is reduced under the drying–wetting cycles (Xu et al. 2021), corresponding to the transformation trend of angular particles to round particles.

3.3 Interpolation equation for collapsibility deterioration

To quantitatively study the deterioration trend of collapsibility under drying–wetting cycles, the collapsibility coefficient δ of compacted loess with 0% salt contents before drying–wetting cycles is set as the zero-deterioration state, the deterioration rate of collapsibility coefficient ($\sim D_\delta$) was introduced and obtained by Eq. (2):

$$D_\delta = \frac{\delta_{ij} - \delta_0}{\delta_0} \tag{2}$$

where δ_0 the value of zero-deterioration state, while δ_{ij} is the value when the number of drying–wetting cycles is i and the salt content is j. According to Eq. (2), the values of D_δ were calculated and shown in Fig. 10.

Figure 10a shows the change in the deterioration rate with salt content ($\sim S$) and the number of drying–wetting cycles ($\sim N$). The value of D_δ increases gradually with an increase in N, but the growth rate gradually slows down, showing deceleration deterioration characteristics. Pronounced intensification occurs in the value of D_δ as S increases, showing accelerated deterioration characteristics. Further, the relationship between deterioration rates with the number of cycles ($D_\delta \sim N$) can be fitted by the hyperbolic function shown in Eq. (3):
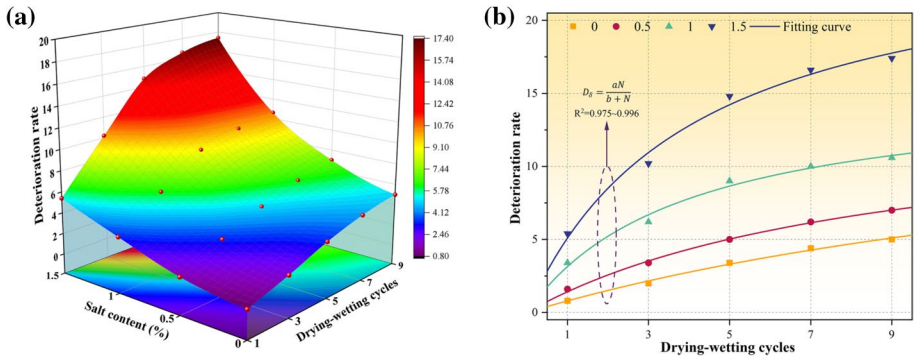
Fig. 10 Deterioration rate of collapsibility coefficient (**a**) $D_\delta \sim N, S$ (**b**) fitting relationship of $D_\delta \sim N$

$$D_\delta = \frac{aN}{b+N}(N > 0) \tag{3}$$

where a and b are both fitting parameters, and the fitting results are shown in Fig. 10b and Table 2. The correlation coefficients R^2 are all in the range of 0.975~0.996, indicating that the hyperbolic function Eq. (3) appropriately models deterioration trend.

The results of D_δ and N were processed as a new relationship between $\frac{N}{D_\delta}$ and N, as shown in Fig. 11. From the fitting results, the relationship between $\frac{N}{V_\delta}$ and N is approximately linear Relationship, i.e.:

$$\frac{N}{D_\delta} = kN + c \tag{4}$$

From Eqs. (3) and (4), $\frac{N}{D_\delta} = \frac{1}{a}N + \frac{b}{a}$ was obtained. Therefore, the ratio of fitting parameters b and a, $\frac{b}{a}$, is the intercept of the line $\frac{N}{D_\delta}$-N, and $\frac{1}{a}$ is the slope of the relationship.
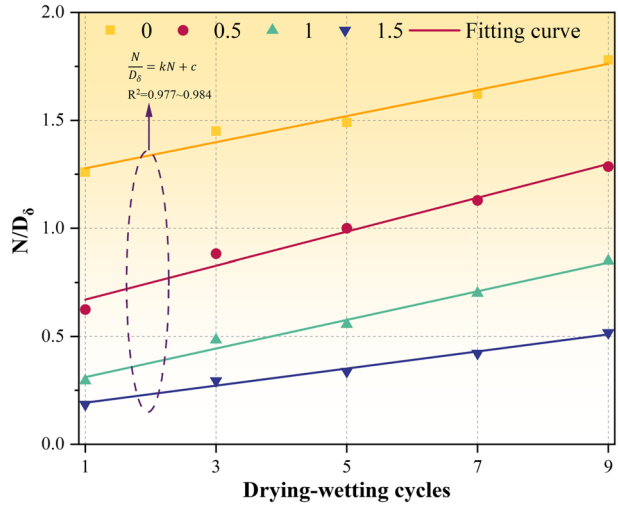
Taking the derivative of Eq. (3) to get:

$$\frac{d(D_\delta)}{dN} = \frac{ab}{(b+N)^2} \tag{5}$$

If $N \to \infty$, Eq. (5) can be transformed into:

Table 2 Fitting parameters at different salt contents

Salt content (%)	Fitting parameters		R^2
	a	b	
0	12.579	19.02	0.996
0.5	13.851	8.787	0.992
1	15.413	4.06	0.977
1.5	25.767	3.907	0.975

Fig. 11 The relationship between $\frac{N}{D_\delta}$ and N

$$\left(D_\delta\right)_{N\to\infty} = a \qquad (6)$$

If N → 0, Eq. (5) can be expressed as:

$$\frac{d(D_\delta)}{dN} = \frac{a}{b} \qquad (7)$$

Thus, the fitting parameter, a, represents the peak value of D_δ when the compacted loess sample reaches the failure limit of the drying–wetting cycles. The ratio of fitting parameters a and b, $\frac{a}{b}$, represents the initial slope of the curve of D_δ~N. In other words, b is the control parameter of deterioration development rate, and the larger d is, the slower the development rate of D_a will be.

Further considering the influence of salt content, Fig. 12 shows the relationship between fitting parameters a, b and salt content, S. One can see that the ultimate deterioration rate (i.e.,
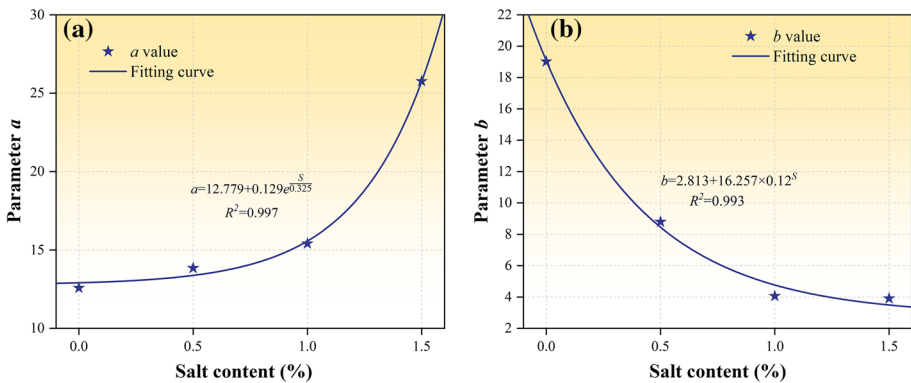

Fig. 12 The relationship between the fitting parameters and the salt content (**a**) $a \sim S$ (**b**) $b \sim S$

a) and the deterioration development speed (i.e., b) are greatly affected by S and the regularity is strong, which can be well described by Eqs. (8)~(9):

$$a = 12.779 + 0.129e^{\frac{S}{0.325}} \tag{8}$$

$$b = 2.813 + 16.257 \times 0.12^{S} \tag{9}$$

The value of a increases from 12.579 to 25.767 as S increases, indicating that soluble salt (i.e., Na_2SO_4) will intensify the deterioration effect of drying–wetting cycles. At the same time, b decreases and gradually tends to be stable as S increases. Furthermore, according to the physical meaning of b, the critical value of N for deterioration saturation will be larger with the increase of S, which in turn shows that decreasing S helps to suppress deterioration caused by drying–wetting cycles.

By substituting Eqs. (8)~(9) into (3), the interpolation equation for collapsibility deterioration of compacted loess with sodium sulfate, considering different drying–wetting cycles and salt content, was obtained:

$$D_\delta(N, S) = \frac{(12.779 + 0.129e^{\frac{S}{0.325}})N}{2.813 + 16.257 \times 0.12^S + N} \tag{10}$$

To verify the applicability of collapsibility deterioration interpolation, the previously stored compacted loess samples with 2, 4, 6 and 8 cycles were assessed for collapsibility coefficient by the double-oedometer test. The test value of D_δ obtained by Eq. (2), and the calculated value obtained by Eq. (10) were compared and are shown in Fig. 13. As can be seen, the correlation coefficient R^2 that is fitted by $y = x$ (i.e., a 1:1 line) between the test and calculated value reaches 0.988, indicating that the interpolation, namely Eq. (10), can well interpolate the collapsibility deterioration of compacted loess with sodium sulfate under drying–wetting cycles.

Fig. 13 Comparison of calculated and test results of D_δ
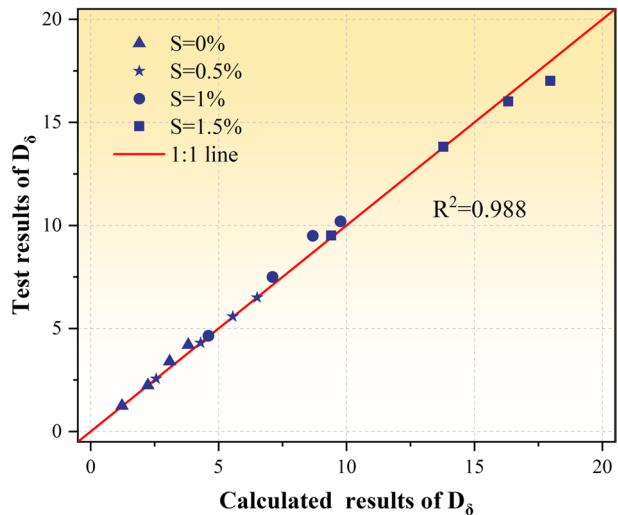
4 Discussion

4.1 Collapsibility deterioration mechanism

The variation of loess collapsibility is the manifestation of the change in loess pore structure at the macroscopic level (Wang et al. 2021b). Combined with the above test results, the collapsibility deterioration mechanism of compacted loess with sodium sulfate under drying–wetting cycles can be analyzed from two aspects: the drying–wetting and salt erosion.

(1) When the loess sample is humidified, the hydration film between loess particles is continuously thickened, thereby increasing the distance between the particles and weakening the bond strength between the particles within the aggregates. While during the dehumidification process, the matric suction in loess sample gradually increases due to continuous water loss (Soulié et al. 2006), which will cause tensile stress on the soil aggregates with weakened bond strength. When the tensile stress reaches a critical value, soil cracking will occur (Tang et al. 2008), which reduces the contact of soil particles (Fig. 6). In the continuous liquid–gas transformation of pore water caused by the drying–wetting, the overall structural strength of compacted loess is weakened and destroyed, and this negative effect is generally irreversible (Yan et al. 2021). It is microscopically manifested as aggregates disintegration, particles movement, and inter-aggregate pores in the loess sample gradually increase under the drying–wetting (shown in Figs. 6 and 15), resulting in macropore and mesopores dominating the pore type (Fig. 9), which provides favorable conditions for the slippage of loess particles during collapsibility (Shao et al. 2018). After several cycles, the overall structure of loess tends to be an equilibrium state (Liu et al. 2015), and the compression space of inter-aggregate pores on which loess collapsibility depends is restricted. Therefore, the increasing trend of loess collapsibility coefficient also gradually slows down with the drying–wetting cycles (Fig. 5a).

(2) Soluble salts (mainly Na_2SO_4) in the loess sample also lead to substantial damage to loess structure. During the dehumidification process of the loess sample, Na_2SO_4 dissolved in the pore water will gradually crystallize into $Na_2SO_4 \cdot 10H_2O$, and the loess particle spacing increases due to salt expansion (shown in Figs. 14 and 15) in that the volume of $Na_2SO_4 \cdot 10H_2O$ is 4.18 times that of Na_2SO_4 (Peng et al. 2019). Then, when the loess sample experiences humidification process, $Na_2SO_4 \cdot 10H_2O$ gradually dissolves in the pore water, resulting in the loss of salt crystallization in the loess framework. The loess particles therefore lose support and this loosening of the loess framework results in further loess structure damage. The repeated crystallization and dissolution of Na_2SO_4 under the drying–wetting cycles weakens the cementation between the compacted loess particles, to the extent that it even disappears. As the salt content of compacted loess sample increases, the loess structure is disturbed more obviously with a large content of macropore and mesopores developed due to the stronger salt expansion (Figs. 7 and 9), which is reflected in the loess collapsibility, that is δ_s will increase with an increase in the Na_2SO_4 content. In the case where there is no drying–wetting cycle (N = 0), the change of Na_2SO_4 content has limited disturbance to the compacted loess structure, because no phase change of Na_2SO_4 occurs at this time, salt erosion cannot occur in the loess sample, causing a limited change in the collapsibility coefficient (Fig. 5b).
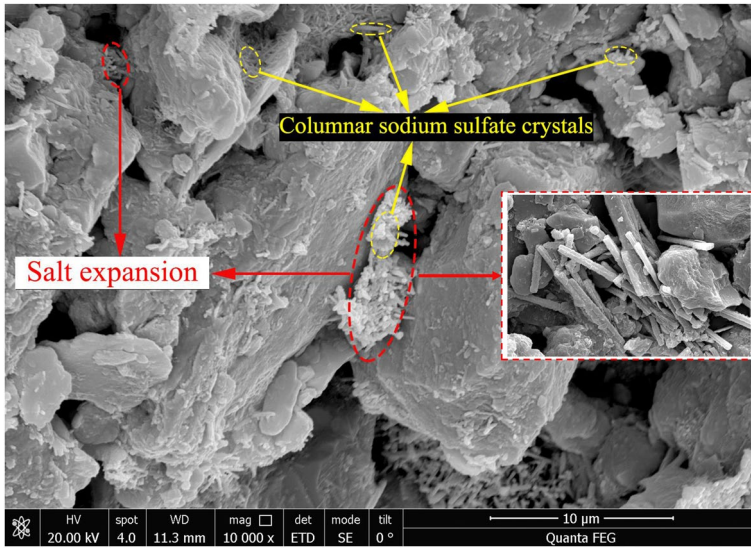
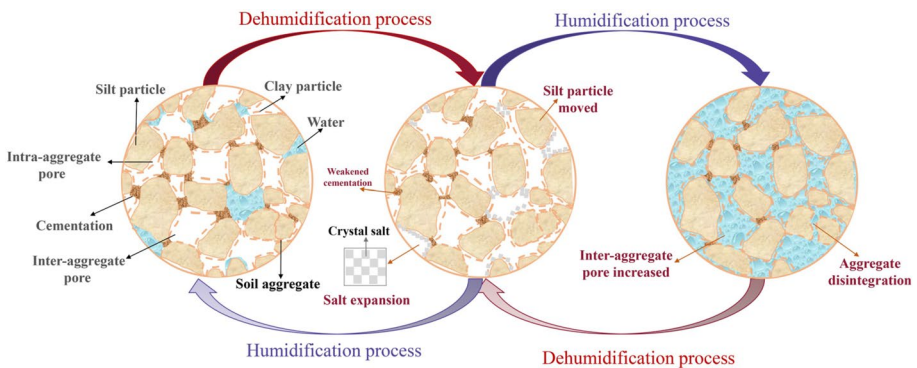**Fig. 14** Sodium sulfate crystals in loess samples

Fig. 15 Microstructure evolution of compacted loess with sodium sulfate under drying–wetting cycles

The combination of the above effects leads to the collapsibility deterioration of compacted loess with sodium sulfate under the drying–wetting cycles.

4.2 Comparison of drying–wetting and salt erosion effect

During the process of drying–wetting cycles, the loess structure is disturbed by the coupled effect of drying–wetting and salt erosion, but the deterioration degree due to each influencing factor is difficult to quantify. Thus, a decoupling analysis of drying–wetting and salt erosion deterioration based on the change in the collapsibility coefficient can be conducted.

Taking the compacted loess under 5 drying–wetting cycles as an example in Fig. 16, the collapsibility deterioration under drying–wetting cycles can be summarized into four typical paths in Fig. 16a, where (i) the a–b path represents the collapsibility deterioration caused only by drying–wetting after 5 cycles; (ii) the b–c path denotes the deterioration due to only salt erosion at 0.5% salt content after 5 cycles; (iii) the b–d path represents the deterioration caused by only salt erosion at 1% salt content after 5 cycles; and (iv) the b–e path denotes the deterioration due to only salt erosion when the salt content is 1.5% after 5 cycles.

Then, the deterioration ratio D_r, as shown in Eqs. (11)~(12), is introduced to separate the deterioration caused by drying–wetting or salt erosion from the total in any path, and the proportion of that caused by each factor is quantified and compared.

$$D_{r1} = \frac{\delta_{i0} - \delta_0}{\delta_{ij} - \delta_0} \qquad (11)$$

$$D_{r2} = \frac{\delta_{ij} - \delta_{i0}}{\delta_{ij} - \delta_0} \qquad (12)$$

In Equations, D_{r1} and D_{r2} are the deterioration ratio due to drying–wetting and salt erosion, respectively; δ_{ij} is the collapsibility coefficient of compacted loess with salt content j after ith drying–wetting cycle; δ_{i0} is the collapsibility coefficient after ith drying–wetting cycle; δ_0 is the initial collapsibility coefficient. Wherein, i is 1, 3, 5, 7 and 9, and j is 0.5%, 1% and 1.5%.

Here, $D_{r1} + D_{r2} = 1$, and the change of both after 5 cycles as shown in Fig. 16b. The value of D_{r1} decreases with an increase in salt content, while the value of D_{r2} increases, showing that under a certain number of cycles, an increase in salt content will cause deterioration associated with drying–wetting to decline, and the proportion of salt erosion gradually increase.

Figure 17 illustrates the ratio of drying–wetting deterioration D_{r1} to salt erosion deterioration D_{r2} under the considered test conditions. One can see that the value of $\frac{D_{r1}}{Dr_2}$ approximately decays exponentially with salt content, which is closely related to the change in the collapsibility coefficient shown in Fig. 5. With higher salt content, the deterioration ratio D_{r2} rises, leading to a reduced value.

In addition, when the salt content is low (S = 0.5%), the value of $\frac{D_{r1}}{D_{r2}}$ is always greater than 1, indicating that the drying–wetting deterioration ratio is higher than that of the salt
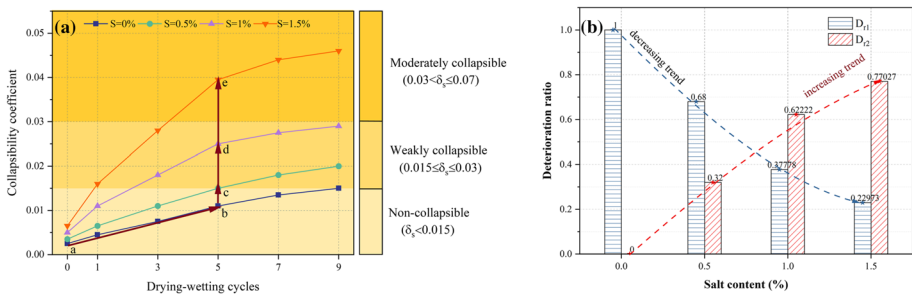

Fig. 16 Schematic diagram of decoupling analysis (**a**) decoupling path (**b**) the change of deterioration ratio
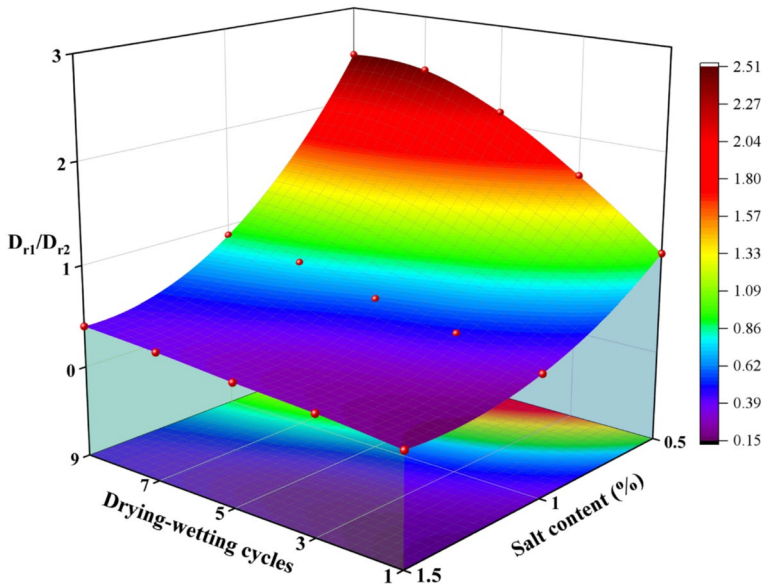
Fig. 17 The ratio of drying–wetting deterioration to salt erosion deterioration

erosion, meaning that the disturbance of drying–wetting on the loess structure is more pronounced compared to salt erosion. This value grows at more drying–wetting cycles, which implies a more significant influence of drying–wetting on loess structure. However, within the range of other salt content considered (S = 1%, 1.5%), the value of $\frac{D_{r1}}{D_{r2}}$ is always less than 1, meaning that the salt erosion causes more disturbance to compacted loess compared to drying–wetting at this specific salt content. Thereby, for the compacted loess with sodium sulfate in Yan'an area, there may exist a critical salinity, S_c, which controls the contribution of drying–wetting and salt erosion to the collapsibility deterioration. When the salt content is higher than S_c, the deterioration of salt erosion on the collapsibility is greater than that of the drying–wetting, that is, the structural damage degree caused by the phase change of soluble salt is higher than that of the pore water; conversely, the collapsibility deterioration of drying–wetting is more significant when the salt content is less than or equal to S_c.

5 Conclusions

In this present paper, the SEM and collapsibility tests were used to comprehensively study the collapsibility deterioration of compacted loess in Yan'an area with sodium sulfate under drying–wetting cycles. The main conclusions are as follows:

(1) The collapsibility of compacted loess samples with sodium sulfate is all deteriorated during drying–wetting cycles condition. The collapsibility coefficient gradually increases and eventually tends to stabilize as the number of drying–wetting cycles increases, while varies with salt content in a linear or exponential pattern.

(2) The microstructure of compacted loess samples shows that after drying–wetting cycles, more micropores and small pores develop into meso- and macropores. Within the considered salt content range, the soil skeleton tends to be loose and the structure tends to weaken, which can be proved by the increase in the fractal dimension of pores and the percentage of inter-aggregate pores area due to the coupling effect of drying–wetting and salt erosion.

(3) According to the fitting analysis of collapsibility test results, the maximum deterioration rate of collapsibility increases exponentially with the increase in salt content, while the development speed gradually decreases. A comprehensive interpolation equation for the collapsibility deterioration of compacted loess was further established considering both cycle numbers and salt content, which can well evaluate the collapsibility deterioration of compacted loess subjected to the coupling effect of drying–wetting and salt erosion.

(4) By decoupling the interaction between drying–wetting and salt erosion, the deterioration ratio caused by each factor was quantitatively analyzed separately. At higher salt contents, the salt erosion deterioration increases while that by drying–wetting decreases. Within the considered range of drying–wetting cycles, when the salt content is higher than 0.5%, the deterioration ratio of salt erosion is always larger than that of drying–wetting, indicating a more obvious influence of salt erosion on the collapsibility of the compacted loess with sodium sulfate.

Declarations

Conflict of interest The authors declare that they have no conflict of interest.

References

Chou Y, Wang L (2021) Soil-water characteristic curve and permeability coefficient prediction model for unsaturated loess considering freeze-thaw and dry-wet. Soils Rocks 44:1–11. https://doi.org/10.28927/SR.2021.058320

Fan X, Xu Q, Scaringia G, Li S, Peng D (2017) A chemo-mechanical insight into the failure mechanism of frequently occurred landslides in the Loess Plateau, Gansu Province, China. Eng Geol 228:337–345. https://doi.org/10.1016/j.enggeo.2017.09.003

Feng S-J, Du F-L, Shi Z-M, Shui W-H, Tan K (2015) Field study on the reinforcement of collapsible loess using dynamic compaction. Eng Geol 185:105–115. https://doi.org/10.1016/j.enggeo.2014.12.006

Higuchi K, Chigira M, Lee D-H, Wu J-H (2015) Rapid weathering and erosion of mudstone induced by saltwater migration near a slope surface. J Hydrol Eng. https://doi.org/10.1061/(ASCE)HE.1943-5584.0001105

Hu M, Liu Y, Ren J, Wu R, Zhang Y (2019) Laboratory test on crack development in mudstone under the action of dry-wet cycles. Bull Eng Geol Env 78:543–556. https://doi.org/10.1007/s10064-017-1080-x

Hu C, Yuan Y, Mei Y, Wang X, Liu Z (2020) Comprehensive strength deterioration model of compacted loess exposed to drying–wetting cycles. Bull Eng Geol Env 79:383–398. https://doi.org/10.1007/s10064-019-01561-8

Ietto F, Perri F, Cella F (2018) Weathering characterization for landslides modeling in granitoid rock masses of the Capo Vaticano promontory (Calabria, Italy). Landslides 15:43–62. https://doi.org/10.1007/s10346-017-0860-5

Jin Z, Guo L, Wang Y, Yu Y (2019) Valley reshaping and damming induce water table rise and soil salinization on the Chinese Loess Plateau. Geoderma 339:115–125. https://doi.org/10.1016/j.geoderma.2018.12.048

Kim D, Kang S-S (2013) Engineering properties of compacted loesses as construction materials. KSCE J Civ Eng 17:335–341. https://doi.org/10.1007/s12205-013-0872-1

Kong L, Sayem HM, Tian H (2017) Influence of drying–wetting cycles on soil-water characteristic curve of undisturbed granite residual soils and microstructure mechanism by nuclear magnetic resonance (NMR) spin-spin relaxation time (T2) relaxometry. Can Geotech J 55:208–216. https://doi.org/10.1139/cgj-2016-0614

Kong F, Nie L, Xu Y, Rui X, He Y, Zhang T, Wang Y, Du C, Bao C (2022) Effects of freeze-thaw cycles on the erodibility and microstructure of soda-saline loessal soil in Northeastern China. CATENA 209:105812. https://doi.org/10.1016/j.catena.2021.105812

Lei X (1987) The types of loess pores in China and their relationship with collapsibility. Sci China B 17:1309–1318

Li G, Ma W, Zhao S, Mao Y, Mu Y (2012) Effect of freeze-thaw cycles on mechanical behavior of compacted fine-grained soil. Cold Reg Eng 2012:72–81

Li P, Vanapalli S, Li T (2016) Review of collapse triggering mechanism of collapsible soils due to wetting. J Rock Mech Geotech Eng 8:256–274. https://doi.org/10.1016/j.jrmge.2015.12.002

Li G, Wang F, Ma W (2018) Variations in strength and deformation of compacted loess exposed to wetting-drying and freeze-thaw cycles. Cold Reg Sci Technol 151:159–167. https://doi.org/10.1016/j.coldregions.2018.03.021

Li X-A, Li L, Song Y, Hong B, Wang L, Sun J (2019) Characterization of the mechanisms underlying loess collapsibility for land-creation project in Shaanxi Province, China-a study from a micro perspective. Eng Geol 249:77–88. https://doi.org/10.1016/j.enggeo.2018.12.024

Liu C, Shi B, Zhou J, Tang C (2011) Quantification and characterization of microporosity by image processing, geometric measurement and statistical methods: application on SEM images of clay materials. Appl Clay Sci 54:97–106. https://doi.org/10.1016/j.clay.2011.07.022

Liu W, Tang X, Yang Q, Li W (2015) Influence of drying/wetting cycles on the mechanical cyclic behaviours of silty clay. Eur J Environ Civ Eng 19:867–883. https://doi.org/10.1080/19648189.2014.974833

Lu H, Li J, Wang W, Wang C (2015) Cracking and water seepage of Xiashu loess used as landfill cover under wetting–drying cycles. Environ Earth Sci 74:7441–7450. https://doi.org/10.1007/s12665-015-4729-4

Luo H, Wu F, Chang J, Xu J (2017) Microstructural constraints on geotechnical properties of Malan Loess: a case study from Zhaojiaan landslide in Shaanxi province, China. Eng Geol 236:60–69. https://doi.org/10.1016/j.enggeo.2017.11.002

Malusis MA, Yeom S, Evans JC (2011) Hydraulic conductivity of model soil–bentonite backfills subjected to wet–dry cycling. Can Geotech J 48:1198–1211. https://doi.org/10.1139/t11-028

Md SH, Ling-wei K, Song Y (2016) Effect of drying–wetting cycles on saturated shear strength of undisturbed residual soils. Am J Civ Eng 4:143–150. https://doi.org/10.11648/j.ajce.20160404.15

Mohurd P (2019) Standard for geotechnical testing method GB/T 50123-2019. China Planning Press, Beijing (In Chinese)

Ni W, Yuan K, Lv X, Yuan Z (2020) Comparison and quantitative analysis of microstructure parameters between original loess and remolded loess under different wetting-drying cycles. Sci Rep. https://doi.org/10.1038/s41598-020-62571-1

Peng S, Wang F, Fan L (2019) Experimental study on influence of vaporous water on salt expansion of sulfate saline soil. Adv Civ Eng. https://doi.org/10.1155/2019/6819460

Pires FL, Auler CA, Roque LW, Mooney JS (2020) X-ray microtomography analysis of soil pore structure dynamics under wetting and drying cycles. Geoderma 362:114103. https://doi.org/10.1016/j.geoderma.2019.114103

Scelsi G, Abed AA, Della Vecchia G, Musso G, Solowski WT (2021) Modelling the behaviour of unsaturated non-active clays in saline environment. Eng Geol. https://doi.org/10.1016/j.enggeo.2021.106441

Shao X, Zhang H, Tan Y (2018) Collapse behavior and microstructural alteration of remolded loess under graded wetting tests. Eng Geol 233:11–22. https://doi.org/10.1016/j.enggeo.2017.11.025

Shen Y, Chen W, Kuang J, Du W (2017) Effect of salts on earthen materials deterioration after humidity cycling. J Central South Univ 24:796–806. https://doi.org/10.1007/s11771-017-3482-0

Soulié F, Cherblanc F, Youssoufi MSE, Saix C (2006) Influence of liquid bridges on the mechanical behaviour of polydisperse granular materials. Int J Numer Anal Meth Geomech 30:213–228. https://doi.org/10.1002/nag.476

Tang C, Shi B, Liu C, Zhao L, Wang B (2008) Influencing factors of geometrical structure of surface shrinkage cracks in clayey soils. Eng Geol 101:204–217. https://doi.org/10.1016/j.enggeo.2008.05.005

Tripathy S, Rao KSS (2009) Cyclic swell-shrink behaviour of a compacted expansive soil. Geotech Geol Eng 27:89–103. https://doi.org/10.1007/s10706-008-9214-3

Wang HB, Zhou B, Wu SR, Shi JS (2011) Characteristic analysis of large-scale loess landslides: a case study in Baoji City of Loess Plateau of Northwest China. Nat Hazard 11:1829–1837. https://doi.org/10.5194/nhess-11-1829-2011

Wang L, Shao S, She F (2019a) A new method for evaluating loess collapsibility and its application. Eng Geol 264:105376. https://doi.org/10.1016/j.enggeo.2019.105376

Wang Z, Fan B, Guo L (2019b) Soil salinization after long-term mulched drip irrigation poses a potential risk to agricultural sustainability: Soil salinization under mulched drip irrigation. Eur J Soil Sci 70:20–24. https://doi.org/10.1111/ejss.12742

Wang F, Li G, Ma W, Mu Y (2020) Effect of repeated wetting-drying-freezing-thawing cycles on the mechanic properties and pore characteristics of compacted loess. Adv Civ Eng 2020:1–8. https://doi.org/10.1155/2020/8839347

Wang H, Ni W, Liu H, Huang M, Yuan K, Li L, Li X (2021a) Study of the repeated collapsibility of undisturbed loess in Guyuan, China. Bull Eng Geol Environ. https://doi.org/10.1007/s10064-021-02304-4

Wang H, Ni W, Yuan K, Li L (2021b) Microstructure evolution of loess under multiple collapsibility based on nuclear magnetic resonance and scanning electron microscopy. J Mt Sci. https://doi.org/10.1007/s11629-021-6838-8

Xu L, Coop M (2016) Influence of structure on the behavior of a saturated clayey loess. Can Geotech J 53:1026–1037. https://doi.org/10.1139/cgj-2015-0200

Xu X, Wang Y, Bai R, Zhang H, Hu K (2016) Effects of sodium sulfate content on mechanical behavior of frozen silty sand considering concentration of saline solution. Res Phys 6:1000–1007. https://doi.org/10.1016/j.rinp.2016.11.040

Xu P, Zhang Q, Qian H, Qu W (2020) Effect of sodium chloride concentration on saturated permeability of remolded loess. Minerals. https://doi.org/10.3390/min10020199

Xu P, Zhang Q, Qian H, Qu W, Li M (2021) Microstructure and permeability evolution of remolded loess with different dry densities under saturated seepage. Eng Geol. https://doi.org/10.1016/j.enggeo.2020.105875

Xue C, Wang X, Liu K (2020) Effect of soaking time and salt concentration on mechanical characteristics of slip zone soil of loess landslides. Water 12:3465. https://doi.org/10.3390/w12123465

Yan C, An N, Wang Y, Sun W (2021) Effect of dry-wet cycles and freeze-thaw cycles on the antierosion ability of fiber-reinforced loess. Adv Mater Sci Eng 2021:8834598. https://doi.org/10.1155/2021/8834598

Yilmaz G, Yetimoglu T, Arasan S (2008) Hydraulic conductivity of compacted clay liners permeated with inorganic salt solutions. Waste Manage Res 26:464–473. https://doi.org/10.1177/0734242X08091586

Ying C, Hu X, Zhou C, Sumi S (2021) Analysis of chemo-mechanical behavior of silty soil under long-term immersion in saline reservoir water. Bull Eng Geol Env 80:627–640. https://doi.org/10.1007/s10064-020-01928-2

Zhang F, Wang G, Kamai T, Chen W (2013) Undrained shear behavior of loess saturated with different concentrations of sodium chloride solution. Eng Geol 155:69–79. https://doi.org/10.1016/j.enggeo.2012.12.018

Zhang Y, Hu Z, Xue Z (2018) A new method of assessing the collapse sensitivity of loess. Bull Eng Geol Env 77:1287–1298. https://doi.org/10.1007/s10064-018-1372-9

Zhang W, Ma J, Tang L (2019) Experimental study on shear strength characteristics of sulfate saline soil in Ningxia region under long-term freeze-thaw cycles. Cold Reg Sci Technol 160:48–57. https://doi.org/10.1016/j.coldregions.2019.01.008

Zhang Y, Hassan MA, King L, Fu X, Istanbulluoglu E, Wang G (2020) Morphometrics of China's Loess Plateau: the spatial legacy of tectonics, climate, and loess deposition history. Geomorphology. https://doi.org/10.1016/j.geomorph.2020.107043